Published in final edited form as:
J Mol Biol. 2007 September 7; 372(1): 194–204. doi:10.1016/j.jmb.2007.06.052.

Molecular basis for Bre5 cofactor recognition by the Ubp3 deubiquitylating enzyme

Keqin Li[1], **Batool Ossareh-Nazari**[3], **Xin Liu**[1,2], **Catherine Dargemont**[3], and **Ronen Marmorstein**[1,2]

1 *The Wistar Institute, University of Pennsylvania, Philadelphia, PA 19104*

2 *Department of Chemistry, University of Pennsylvania, Philadelphia, PA 19104*

3 *The Institute Jacques Monod, UMR7592 CNRS/Paris VI/Paris VII, 75251 Paris, France*

SUMMARY

Yeast Ubp3 and its co-factor Bre5 form a deubiquitylation complex to regulate protein transport between the endoplasmic reticulum and Golgi compartments of the cell. A novel N-terminal domain of the Ubp3 catalytic subunit forms a complex with the NTF2-like domain of the Bre5 regulatory subunit. In this study, we report the X-ray crystal structure of an Ubp3/Bre5 complex and show that it forms a symmetric hetero-tetrameric complex in which the Bre5 NTF2-like domain dimer interacts with two L-shaped β-strand-turn-α-helix motifs of Ubp3. The Ubp3 N-terminal domain binds within a hydrophobic cavity on the surface of the Bre5 NTF2-like domain subunit with conserved residues within both proteins interacting predominantly through anti parallel β-sheet hydrogen bonds and van der Waals contacts. Structure-based mutagenesis and functional studies confirm the significance of the observed interactions for Ubp3-Bre5 association *in vitro* and Ubp3 function *in vivo*. Comparison of the structure to other protein complexes with NTF2-like domains shows that the Ubp3/Bre5 interface is novel. Together, these studies provide new insights into Ubp3 recognition by Bre5 and into protein recognition by NTF2-like domains.

Keywords

Protein-protein recognition; Deubiquitylation; ubiquitin-specific processing proteases (UBPs); nuclear transfer factor 2 (NTF2)-like domain

INTRODUCTION

Deubiquitylation is catalyzed by deubiquitylating proteases (DUBs) that fall into at least five distinct families: the ubiquitin-specific processing proteases or UBPs; the ubiquitin carboxy-terminal hydrolases UCHs; the Ataxin-3/Josephin domains; the Ovarian Tumor domain-containing proteases or OTUs and the JAMM proteases [1]. Among these DUB families, the UBPs (also called USPs in human) represent the most widespread deubiquitylating enzymes across evolution and have been implicated to regulate diverse biological processes [1]. Homology among the UBP enzymes is restricted to a roughly 350-residue catalytic core

Correspondence should be addressed to Ronen Marmorstein, The Wistar Institute Philadelphia, PA 19104. e-mail: E-mail: marmor@wistar.org.

domain, while the UBPs contain variable N terminal, or occasionally, C-terminal extensions, or insertions in the catalytic domains. The molecular basis for how different UBPs select their cognate substrates and mediate distinct cellular functions is still unclear, although the variable N-and C- terminal extensions, association with different cofactor proteins [2; 3], and subcellular localization [4; 5] have been implicated in the process.

The structure of the catalytic domain of the UBPs both alone and in complex with ubiquitin [6], and of other regions of the UBPs in complex with regions of their protein substrates [7; 8; 9] have provided important information underlying the catalytic activity of these enzymes and their mode of substrate targeting. In contrast, there has been no structural information reported to date on a deubiquitylating enzyme in complex with its protein cofactor, and therefore the structural basis for cofactor recognition by ubiquitylating enzymes has remained obscure.

One such Ubp/cofactor complex is the Ubp3/Bre5 complex. Ubp3, the yeast homologue of human USP10, has been shown to form a complex with the Bre5 cofactor to specifically deubiquitylate and consequently control the expression level of the Sec23 [10] and β ′-COP [11] subunits of the COPII and COPI complexes that regulate anterograde and retrograde transport between the endoplasmic reticulum (ER) and the Golgi apparatus [10], respectively. Deubiquitylation by the Ubp3/Bre5 complex has also been shown to play a role in cytoplasm to vacuole (Cvt) trafficking. The substrate for the Ubp3/Bre5 complex in this pathway is the cargo receptor, Atg19p, whose ubquitylation status is a functional component in the Cvt pathway [12]. We previously showed that Bre5 is an essential positive regulator for Ubp3-mediated biological function in vivo [10]. However, Bre5 does not complement a catalytically inactive Ubp3 and is not involved in substrate recognition[10]. Current hypotheses suggests that Bre5 could influence either the targeting of Ubp3 to its specific substrate, or modulate its catalytic activity or both.

Yeast Bre5 has two recognizable domains, a nuclear transfer factor 2 (NTF2)-like domain at the N terminus (residues 8–140) and a RNA recognition motif (RRM) at the C terminus (residues 419–481) (Figure 1A). Although, NTF2-like domains are found in many proteins with diverse activities, [13; 14; 15; 16], a common function of these domains appears to be that they mediate protein-protein interactions. In previous structure/function studies, we showed that the Bre5 NTF2-like domain forms a tightly associated homodimer that directly associates, also with high affinity, with a folded domain within the N-terminus of Ubp3 [17]. In contrast the RRM is not required for the function of the Bre5/Ubp3 complex at least on Sec23 and β′-COP substrates[11].

Yeast Ubp3 is a 912 amino acid residues protein. The C terminal half of Ubp3 (450–912) harbors the UCH (Ubiquitin carboxyl-terminal hydrolase) catalytic domain, while the N-terminal half has no detectable sequence homology to other proteins (Figure 1A). Our previous study showed that residues 180–260 within the N-terminal half of Ubp3 harbors a Bre5 binding domain [17].

In this study, we present the X-ray crystal structure of the Bre5 NTF2-like domain in complex with a high affinity N-terminal domain of Ubp3 (residues 189–233), that shows that the Ubp3 N-terminal domain adopts a novel L-shaped β-sheet-turn-α-helix topology that interacts with the Bre5 NTF2-like domain in a mode that differs from other protein complexes with NTF2-like domains. We also perform structure-based mutagenesis and functional studies to confirm the significance of the observed Ubp3/Bre5 complex for Ubp3-cofactor association *in vitro* and Ubp3 function *in vivo*. Together, these studies provide new insights into Ubp3 recognition by Bre5 and into protein recognition by NTF2-like domains.

RESULTS AND DISCUSSION

Overall structure of the Ubp3/Bre5 hetero-tetramer complex

We used X-ray crystallography to determine the high resolution structure of the NTF2-like domain of Bre5 (Bre5-NTF2, residues 1–146) in complex with an N terminal high affinity binding domain of Ubp3 (residues 189–233, called Ubp3-Nterm to distinguish it from the C-terminal Ubp3 catalytic domain). The crystals form in the space group $P2_12_12_1$ with 2 subunits each of Bre5-NTF2 and Ubp3-Nterm per asymmetric unit cell. The structure was determined by molecular replacement using Bre5-NTF2 as a search model [17] and refined to 1.7Å resolution with good refinement statistics and geometry (Table 1).

Bre5-NTF2 forms a tightly associated homodimer with each Bre5-NTF2 subunit interacting with a domain of Ubp3-Nterm (Figures 1B and 1C). The Bre5-NTF2 dimer in the Ubp3/Bre5 complex adopts a mixed α/β fold that is similar to the free Bre5-NTF2-like domain and other NTF2-like domains. Briefly, each Bre5-NTF2 subunit contains a 6-stranded (β1–β6) anti-parallel β sheet that forms a curved platform for three α helices (α1–α3) that lie on the concave side of the β-sheet. The dimer interface is formed along the convex surfaces of the β-sheets from each of the subunits such that residues from β1 and β3–β6 mediate both hydrogen bond and van der Waals contacts.

The Ubp3-Nterm domain forms a 3-residue loop, followed by a 7-residue β1-strand, sharp turn and a 15-residue α1-helix (Figures 1B and 1C). The strand and helix are nearly perpendicular to each other forming an L-shape. Residues 190–205 of Ubp3-Nterm, N-terminal to the 3 residue loop could not be traced into the electron density map and are presumably disordered.

The Ubp3-Bre5 interface

Bre5-NTF2 and Ubp3-Nterm form nearly symmetrical interactions within the heterotetramer. These interactions are predominantly hydrophobic in nature and can be separated into two distinct regions of contact; between the Ubp3-Nterm β1-sheet-turn with the β3-sheet and α1-helix of Bre5-NTF2, and between the N-terminal half of the α1-helix of Ubp3-Nterm with the L2 loop (β4– β5 turn) and, to a lesser extent, the L1 loop (β1– β2 turn) of Bre5-NTF2 (Figure 2A).

Ubp3-Nterm β1 residues 208–210 form anti-parallel β-sheet hydrogen bonds with the Bre5-NTF2 β3 residues 81–83. The side chains of Ubp3-Nterm β1 residues Leu 208, Phe209, Ile 210, Asn 211 and Phe 212 also make a series of side chain van der Waals interactions with several residues in the β3-strand (Lys 80, Leu 81, Lys 82 and Leu 83) and α1-helix (Pro 10, Gln 14, Tyr 17, Glu 18 and Arg 21) of Bre5-NTF2 (Figure 2B). In the turn that proceeds the β1 sheet of Ubp3-Nterm, Phe 217 also makes a van der Waals contact with the aliphatic region of Lys 82 of Bre5-NTerm and Ubp3-term Glu 216 makes the only side chain hydrogen bond in this region with Bre5-NTF2 Lys 80 (Figure 2B).

The Ubp3-Nterm α1-helix also makes predominantly van der Waals contacts with the L1 and L2 loops of Bre5. Residues Ala 220, Ser 221, Gln 223 and Arg 224 of Ubp3-Nterm make extensive van der Waals interactions with the L2-loop residues Pro 112, Val 113 and Tyr 114 of Bre5-NTF2 (Figure 2C). The side chain Arg 224 nitrogens of Ubp3-Nterm also makes a hydrogen bond with the main chain of Val 113 within the Bre5-NTF2 L2 loop as well as hydrogen bond and van der Waals contacts with Asp residues 51 and 52, respectively, within the L1-loop of Bre5-NTF2 (Figure 2C).

A sequence alignment of Ubp3-Nterm with other yeast Ubp3 homologues shows high sequence conservation of residues in the β1-turn-α1 region that contact Bre5-NTF2 (Figures 2C and 2D). In particular, this region shows the highest conservation outside of the catalytic domain and

the majority of the residues that mediate Bre-NTF2 contacts are either strictly or highly conserved within the yeast Ubp3 homologues (Figure 2D). Not surprisingly, the residues in Bre5-NTF2 that mediate Ubp3 contacts are also highly conserved within the yeast Bre5 homologues (Figure 2C). Taken together, these findings suggest that the yeast Ubp3 homologues adopt a similar β1-turn-α1 structure and mediate analogous contacts with their corresponding Bre5 homologues. Interestingly, only part of the yeast Ubp3 conservation extends to the Ubp10 human ortholog (Figures 2C and 2D). In particular, of the Ubp3 residues that contact Bre5, only Pro 207, Val 210, Glu 216 and Phe 217 show conservation, suggesting that the yeast-specific Ubp3-Bre5 interaction may differ in human.

A comparison of the Ubp3-Nterm/Bre5-NTF2 complex with the free Bre5-NTF2 domain shows that, except for the L1 and L2 loops, the Bre5 dimer is essentially superimposable with an RMSD of 1.1Å for all atoms of Bre5 (Figure 3A). Importantly, the conformational changes within the L1 and L2 loops of Bre5 appear to be correlated with Bre5 interaction with Ubp3. In particular, in the absence of Ubp3 binding, the L1 loop appears flexible with 12 residues (43 to 54) untraceable in the electron density map. In the presence of Ubp3-Nterm, this loop becomes more ordered with only 4 residues (46 to 49) untraceable in the electron density map of the complex and residues Asp 51 and Asp52 of the L1 loop make contacts to Arg 24 within the α1-helix of Ubp3.

The L2 loop of the Bre5-NTF2 domain undergoes the most dramatic structural shift upon Ubp3-Nterm binding and this movement appears to be directly coupled to complex formation. In particular, in the absence of Ubp3-Nterm, this loop and the ends of the β-sheets that form it are flipped away from the body of the rest of the Bre5-NTF2 protein. Indeed, this “flipped out” conformation would prevent Ubp3-Nterm binding due to steric occlusion (Figure 3A). In the Ubp3-Nterm/Bre5-NTF2 complex, this loop flips inward by about 5 Å toward the body of the protein and forms part of the binding pocket for Ubp3-Nterm (Figure 3B). The movement of this loop in the Bre5-NTF2 domain not only helps create a binding site for Ubp3-Nterm but residues Pro 112, Val 113 and Tyr 114 of the loop also directly participate in interactions with the α1-helix of Ubp3-Nterm, as described above. Conservation of Pro 112 and Tyr 114 of the L2 loop and Asp 52 of the L1 loop suggests that the L1 and L2 loops of Bre5 may play important roles in Ubp3 association.

Structure-based mutagenesis of the Ubp3-Bre5 interface

To probe the functional importance of the Ubp3-Bre5 interface observed in the crystal structure we carried out structure-based mutagenesis. We initially prepared single alanine replacements of several Bre5 and Ubp3 residues shown to mediate protein-protein interactions in the complex and used GST-pulldown studies to compare the protein binding properties of these mutants. Specifically, using wild-type and single alanine GST-tagged Ubp3-Nterm mutants (L208, F209, I210, N211, T212, E216, F217 and R214), we carried out pull down studies with the wild-type Bre5-NTF2 domain. We also carried out analogous pull down studies with wild-type GST-Ubp3-Nterm and several single alanine His-Bre5-NTF2 mutants (Y17, K80, K82 and E105). As can be seen in figure 4A, only the single I210A Ubp3 mutation showed reduced binding relative to wild-type levels.

Since the I210A Ubp3 mutation was not sufficient to abolish binding, we next prepared proteins containing multiple mutations and assayed protein binding using pull down studies as described above. The results of these pull down studies are shown in figure 4B with a summary of the mutants that were tested and their binding properties in table 2. Mutations of residues I208, F209, I210, N211 and F217 in Ubp3 in any combination significantly reduce binding to Bre5. Together, these results reinforce the structural findings that the β1-α1 helix of Ubp3-Nterm plays an important role in Ubp3-Bre5 association.

To obtain more quantitative information underlying the interaction between Upb3 and Bre5 we carried out an Isothermal Titration Calorimetry study. For these studies we produced in bacteria a near full-length Ubp3 construct that contained both the Bre5 interaction domain and the catalytic domain (residues 189–912) and the NTF2 domain of Bre5. This analysis revealed that Bre5 and Ubp3 interact very strongly with a dissociation constant of 119 nM (Figure 4C). We also prepared an Ubp3 (189–912) mutant containing alanine substitutions at the following residues: L208, F209, I210, N211 and F217 for ITC studies with the wild-type Bre5-NTF2 and could not detect binding using analogous conditions (Figure 4C). This comparison, in combination with our structural findings, reported here, is consistent with our conclusion that the β1-α1 region of the Ubp3-Nterm is necessary and sufficient for tight Bre5 association.

In an earlier study, we showed that the same NTF2 domain of Bre5 interacts with an N-terminal Ubp3 (181–282) construct with a dissociation constant of 187 nM, simlilar to that reported here but with a Bre5-NTF2/Ubp-Nterm stochiometry of 2:1 instead of the 1:1 stociometry reported here [17]. Although the Bre5-NTF2 domain used in both studies are the same, the Ubp construct differs. While the earlier studies employed the shorter Ubp3 (181–282) construct, the present study employed the longer Ubp3 (189–912) construct that also includes the C-terminal catalytic domain of Ubp3 (Figure 1A). Although, we do not know the reason for this discrepancy, we hypothesize that other regions of Ubp that are outside of the N-term region that is shown in the crystals to contact the Bre5 NTF2-like domain, contributes to 1:1 stoichiometric Bre5/Ubp association. The high concentration of Bre5-NTF2 and Ubp-Nterm in the crystals may shift the equilibrium to the 1:1 stochiometry, despite the absence of other regions of Ubp3 that might contribute to Bre5/Ubp3 complex formation. Alternatively, a subset of the shorter Ubp3 (181–282) pool of the earlier study might have been improperly folded (consistent with our inability to produce a recombinant Ubp3 (189–233) construct in soluble form, data not shown), thus reducing the pool of Ubp3 available for Bre5-NTF2 binding. Also in an earlier study, we showed that Y42R and R139F mutations in the NTF2-like domain of Bre5 disrupted Upb3 binding *in vitro* and Ubp3 function *in vivo* and we had proposed that these residues might be directly involved in Ubp3 interaction. In the current structure, we see that these residues are not directly involved in Ubp3 interaction and thus hypothesize that since they are partially buried in the current structure (Y42 making intraatomic contacts and R139 making interatomic contacts) that their mutational properties may be due to a partial disruption of the Bre5 dimer structure that is required for Ubp 3 binding. Taken together, the structure of the Bre5/Ubp3 complex reported here now provides a scaffold from which to understand these earlier results.

In vivo analysis of Bre5p/Ubp3 interaction and function

To confirm that the Bre5 and Ubp3 interface characterized *in vitro* is also responsible for *in vivo* interaction and function of the Bre5/Ubp3 complex, we analyzed the ability of wild-type and interaction mutants of Bre5 and Ubp3 to interact and mediate deubiquitylation in cells. For this purpose, His-tagged versions of wild type or mutant Bre5 were introduced into Ubp3-HA/*bre5Δ* cells as previously described [11; 17]. The ability of wild-type and mutant Bre5 protein to interact with endogenous Ubp3 was measured by co-immunoprecipitation using anti-HA antibodies followed by western blotting (Figure 4D, top panel). The function of the complex between Ubp3 and wild-type or mutant Bre5 was also followed by the capacity of the protein complex to mediate deubiquitylation of Sec23, a substrate for the Bre5/Ubp3 deubiquitylation complex (Figure 4E, top panel). In addition, His-tagged versions of wild type or mutant Ubp3 were introduced into Bre5-GFP/*ubp3Δ* cells (Figure 4D and 4E, lower panel) and the extent of Ubp3-Bre5 interaction was also followed both by co-immunoprecipitation using anti-GFP antibodies and the capacity of the complex to mediate deubiquitylation of Sec23. As shown in Figures 4D and 4E, expression of wild type Bre5 or Ubp3 was able to form a complex with their endogenous counterpart and restore the deubiquitylation of Sec23 in *bre5Δ* and *ubp3Δ*

cells, respectively. However, in agreement with the *in vitro* interaction studies (Figure 4B), a Bre5 mutant harboring both Y17A and K82A mutations displayed a modest (2–3 fold) but reproducible decrease in its binding to Ubp3 (Figure 4D, top panel) and showed a fairly small, but detectable, decrease in sec23 deubiquitylation (Figure 4E, top panel). In addition, the Ubp3 mutant harboring the L208A, F209A, I210A, and N211A substitutions was severely deficient in its interaction with Bre5 (Figure 4D, bottom panel) and led to a more dramatic decrease in sec23 deubiquitylation (Figure 4E, bottom panel). Significantly, these *in vivo* results mirror the *in vitro* binding studies showing that both the Bre5 Y17A/K82A but mainly the Ubp3 L208A/F209A/I210A/N211A mutants decrease Bre5-Upb3 association (Figure 4B and Table 2). Taken together, these results demonstrate that association between Bre5 and Ubp3 through the interface defined in the crystal structure reported here is important for Ubp3 function *in vivo*.

Comparison of the Bre5/Ubp3 interface to other protein complexes with NTF2 domains

It is somewhat striking that the NTF2-like domains adopt highly homologous dimeric structures given the rather low but significant sequence homology (Figure 5). One potential reason for the low sequence homology may be due to the fact that different NTF2-like domains exploit this sequence divergence to interact with different cognate proteins. A comparison of the Ubp3/Bre5 complex reported here with other protein complexes with NTF2 and other NTF2-like domains reveals that this is indeed the case. Specifically, while Ran GTPase interacts with its cognate NTF2 dimer on the same “top” surface as Ubp3 of the NTF2 dimer, Ran GTPase uses two loop regions to interact with loop regions on the opposite face of the top surface of the NTF2 dimer (Figures 5A and 5B) [18]. Interestingly, the TAP subunit of the TAP/P15 heterodimer contains an extra C-terminal helix that sits at the dimer interface of the top surface of the NTF2-like dimer contributing to specificity of the NTF2 domain heterodimer [15; 16; 19]. In contrast, the nucleoporin FG repeat loop interacts with loops in the “bottom” surface of the TAP/P15 dimer (Figures 5A and 5B) [13; 15]. Taken together, it appears that the NTF2-like domains employ sequence divergence, predominantly within loop regions, on different surfaces to specifically associate with their cognate proteins. The Ubp3/Bre5 complex represents yet another example of how different NTF2-like domains form protein-specific recognition modules to modulate distinct biological processes.

EXPERIMENTAL PROCEDURES

Protein preparation

The Ubp3 gene was amplified by PCR from yeast genomic DNA and inserted into the pGEX5T expression vector. A construct encoding residues 190–233 of Ubp3 (Ubp3-Nterm) was subcloned by PCR into the PGEX4T-1 expression vector for the preparation of the GST-Ubp3 (190–233) fusion protein. The longer Ubp3(189–912) construct that includes both the N-terminal Bre5 binding domain and the catalytic deubiquitylation domain was subcloned by PCR into the pET28A expression vector for preparation of a C-terminal 6xHis fusion protein. DNA encoding residues 1–146 of Bre5 (Bre5-NTF2) was PCR amplified from yeast genomic DNA and subcloned into the pET28-A expression vector for preparation of the 6x-His-Bre5 (1–146) fusion protein.

All Ubp3 and Bre5 expression plasmids were transformed or co-transformed into E. coli strain BL21 (DE3) for protein expression. Transformed bacteria were initially grown at 37° C to an absorbance of 0.7–0.9 at 600 nm, and protein was overexpressed by addition of 0.1mM IPTG followed by overnight growth at 15 °C. Cells were disrupted by sonication in a solution containing PBS buffer supplemented with 10mM BME and 1mM PMSF. For the purification of His-tagged fusion proteins, the respective protein was partially purified using a Ni-NTA resin as described by the manufacturer and further purified using cation exchange (SP-

Sepharose) and gel filtration (Superdex-75) chromatography in PBS buffer. For purification of GST-Ubp3(190–233), the supernatant was partially purified using glutathione resin (Novagen) as described by the manufacturer.

For preparation of the Ubp3-Nterm/Bre5-NTF2 complex for cocrystallization, the proteins were co-expressed of their expression plasmids in BL21 (DE3) cells as described above. The cell lysate was loaded onto a Ni-NTA resin (to capture the complex using the C-terminal 6xHis-tag on Bre5), washed with buffer (20mM Hepes, PH7.0, 300 mM NaCl, 10mM BME) and eluted with a gradient of 15–300 mM imidazole in the same buffer.

Fractions containing Ubp3/Bre5 complex were loaded onto a GST resin (to capture the complex using the N-terminal GST tag on Upb3). Both the GST and 6x-His tags were removed by treating a slurry of the resin-bound complex with thrombin (10 U/mg fused protein) overnight at 4°C, and the untagged complex was eluted with buffer (20mM Hepes, PH7.0, 150 mM NaCl, 10mM BME). The complex was further purified with gel filtration (Superdex-75) chromatography in the same buffer. Protein purity was judged to be greater than 90% by SDS-PAGE and the protein was concentrated to 10–20 mg/ml for crystallization.

Site-directed protein mutants were prepared using the Quick Change Mutagenesis kit essentially as described by the manufacturer (Stratagene), the sequence of the mutants confirmed by sequencing and the mutant proteins were purified essentially as described for the wild-type protein proteins.

Crystallization and structure determination

Crystals of the Ubp3-Nterm/Bre5-NTF2 complex were grown at room temperature using the hanging drop vapor diffusion method. 2 ul of protein solution at 14 mg/ml in 20 mM HEPES, pH 7.0, 10mM BME and 150 mM NaCl was mixed with an equal volume of reservoir solution containing 10% PEG 20,000, 100 mM Bicine, pH 9.0, 2% Dioxan and equilibrating over 0.5 ml of reservoir solution. Crystals grew to a typical size of 500×100×50 μm over 5 days and were flash frozen in a reservoir solution supplemented with 20% glycerol for storage in solid propane prior to data collection.

Single wavelength native data were collected on beamline F1 at the CHESS using an ADSC Quantum-4 CCD detector at 100K. The data were processed with the HKL 2000 suite (HKL Research Inc.) and the relevant statistics are summarized in Table 1. The structure of the complex was determined by molecular replacement with the program Molrep [20], using the Bre5(1–146) protein structure (PDB 1ZX2, [17]) as a search model. Model refinement employed simulated annealing and torsion angle dynamic refinement protocols in CNS with iterative manual adjustments of the model using the program O, with reference to 2Fo-Fc and Fo-Fc electron density maps. Solvent molecules were modeled into the electron density map using the programs CNS and ARP/wARP [21; 22] and the later stages of refinement was carried out using translation, liberation, and screw-rotation (TLS) and restraint refinement in the program REFMAC5 [23]. The final model was checked for errors with a composite-simulated annealing omit map and showed excellent refinement statistics and geometry (Table 1).

In vitro Ubp3-Bre5 binding studies

For pull-down assays, GST-Ubp3 (190–233) protein (50 μM in PBS buffer) was incubated with purified His-Bre5(1–146) (50 μM in PBS buffer) for 1 h at 4°C, followed by immobilization on 30μl glutathione–Sepharose beads for 1 h at 4°C. Beads were washed 3 times with 1ml PBS buffer and 5–10 ul aliquots were mixed with an equal volume of 2x SDS-loading buffer and analyzed on SDS–PAGE.

Isothermal Titration Calorimetry (ITC) measurements were carried out using a MicroCal VP-ITC isothermal titration calorimeter (MicroCal, Inc) and each experiment was carried out in duplicate. Wild-type or mutated Ubp3(189–912) was diluted to 30 μM in PBS buffer and added to a 1.4 ml sample cell, and a 0.3 mM solution of wild-type Bre5(1–146) protein titrant was loaded into the injection syringe. For each titration experiment, a 60 sec. delay at the start of the experiment was followed by 30 injections of 10μl of the titrant solution. The sample cell was stirred at 300 rpm throughout and maintained at 15°C. Titration data were analyzed using the Origin 5.0 software supplied by MicroCal Inc. and data sets were corrected for baseline heats of dilutions from control runs as appropriate. The corrected data was then fit to a theoretical titration curve describing one binding site per titrant. The area under each peak of the resultant heat profile was integrated and plotted against the molar ratio of Ubp3 to Bre5. A non-linear best-fit binding isotherm for the data was used to calculate Ubp3/Bre5 stoichiometry, dissociation constant and standard enthalpy change.

In vivo analysis of Sec23 ubiquitylation state

Yeast cultures were grown either in rich medium (YPD; Q-Biogen) or in minimal medium (SD) containing 0.67% yeast nitrogen base with ammonium sulfate, 2% dextrose, and supplemented with appropriate nutrients [24]. Yeast transformations were performed using standard procedures and preparation of the *Bre5Δ* and *Ubp3Δ* strains were as previously described [11]. The point mutations in Bre5-His Y17K82A and Ubp3-His L208F209I210N211A were prepared with appropriate primers, p426-ADH-Bre5-His and p423-ADH-Ubp3-His plasmids as template respectively and the QuickChange mutagenesis kit (Stratagene).

Yeast cells grown in YPD or minimal medium were collected during the exponential growth phase (OD 600nm of 2 or 0.8 respectively). Total protein extracts were prepared by the NaOH-TCA lysis method [10]. Protein samples were separated by 7% SDS-PAGE, transferred to nitrocellulose membranes, probed with appropriate antibodies, and detected with chemiluminescence protein immunoblotting reagents (Pierce). Rabbit polyclonal antibodies to Sec23p (1:400 dilution), were kindly provided by B. Lesch and R. Schekman, and mouse monoclonal antibody anti-His was purchased from Santa Cruz Biotechnology.

Co-Immunoprecipitation experiments

Yeast cells were grown up to an OD_{600}= 1.2. Cells were harvested and lysed at 4°C with glass beads in ice-cold IP buffer [10]. The lysate was centrifuged for 30 min at 13000g. The supernatant was incubated with protein G–Sepharose beads (Amersham) and antibodies for 2h at 4 °C. Beads were then washed with IP buffer and bound proteins were eluted by heating samples at 95°C for 5 min in Laemmli sample buffer before Western-blot analysis using anti-HA (Babco), anti-His (Santa Cruz) or anti GFP (Roche) antibodies.

Acknowledgements

This work was supported by NIH grants to R.M., by a grant from the Commonwealth Universal Research Enhancement Program, Pennsylvania Department of Health awarded to the Wistar Institute and the Minister for Research and the Association de Recherche contre le Cancer grants to C.D. Coordinates for the Ubp3(190–233)/Bre(1–146) complex structure has been deposited to the Rutgers Collaborative Structural Bioinfomatics database under accession number XXXX.

REFRENCES

1. Nijman SM, Luna-Vargas MP, Velds A, Brummelkamp TR, Dirac AM, Sixma TK, Bernards R. A genomic and functional inventory of deubiquitinating enzymes. Cell 2005;123:773–86. [PubMed: 16325574]

2. Papa FR, Amerik AY, Hochstrasser M. Interaction of the Doa4 deubiquitinating enzyme with the yeast 26S proteasome. Mol Biol Cell 1999;10:741–56. [PubMed: 10069815]
3. Wilkinson KD. Ubiquitination and deubiquitination: targeting of proteins for degradation by the proteasome. Semin Cell Dev Biol 2000;11:141–8. [PubMed: 10906270]
4. Lin H, Yin L, Reid J, Wilkinson KD, Wing SS. Divergent N-terminal sequences of a deubiquitinating enzyme modulate substrate specificity. J Biol Chem 2001;276:20357–63. [PubMed: 11278432]
5. Lin H, Keriel A, Morales CR, Bedard N, Zhao Q, Hingamp P, Lefrancois S, Combaret L, Wing SS. Divergent N-terminal sequences target an inducible testis deubiquitinating enzyme to distinct subcellular structures. Mol Cell Biol 2000;20:6568–78. [PubMed: 10938131]
6. Hu M, Li P, Li M, Li W, Yao T, Wu JW, Gu W, Cohen RE, Shi Y. Crystal structure of a UBP-family deubiquitinating enzyme in isolation and in complex with ubiquitin aldehyde. Cell 2002;111:1041–54. [PubMed: 12507430]
7. Hu M, Gu L, Li M, Jeffrey PD, Gu W, Shi Y. Structural basis of competitive recognition of p53 and MDM2 by HAUSP/USP7: implications for the regulation of the p53-MDM2 pathway. PLoS Biol 2006;4:e27. [PubMed: 16402859]
8. Saridakis V, Sheng Y, Sarkari F, Holowaty MN, Shire K, Nguyen T, Zhang RG, Liao J, Lee W, Edwards AM, Arrowsmith CH, Frappier L. Structure of the p53 binding domain of HAUSP/USP7 bound to Epstein-Barr nuclear antigen 1 implications for EBV-mediated immortalization. Mol Cell 2005;18:25–36. [PubMed: 15808506]
9. Sheng Y, Saridakis V, Sarkari F, Duan S, Wu T, Arrowsmith CH, Frappier L. Molecular recognition of p53 and MDM2 by USP7/HAUSP. Nat Struct Mol Biol 2006;13:285–91. [PubMed: 16474402]
10. Cohen M, Stutz F, Belgareh N, Haguenauer-Tsapis R, Dargemont C. Ubp3 requires a cofactor, Bre5, to specifically de-ubiquitinate the COPII protein, Sec23. Nat Cell Biol 2003;5:661–7. [PubMed: 12778054]
11. Cohen M, Stutz F, Dargemont C. Deubiquitination, a new player in Golgi to endoplasmic reticulum retrograde transport. J Biol Chem 2003;278:51989–92. [PubMed: 14593109]
12. Baxter BK, Abeliovich H, Zhang X, Stirling AG, Burlingame AL, Goldfarb DS. Atg19p ubiquitination and the cytoplasm to vacuole trafficking pathway in yeast. J Biol Chem 2005;280:39067–76. [PubMed: 16186126]
13. Bayliss R, Leung SW, Baker RP, Quimby BB, Corbett AH, Stewart M. Structural basis for the interaction between NTF2 and nucleoporin FxFG repeats. Embo J 2002;21:2843–53. [PubMed: 12065398]
14. Bullock TL, Clarkson WD, Kent HM, Stewart M. The 1.6 angstroms resolution crystal structure of nuclear transport factor 2 (NTF2). J Mol Biol 1996;260:422–31. [PubMed: 8757804]
15. Fribourg S, Conti E. Structural similarity in the absence of sequence homology of the messenger RNA export factors Mtr2 and p15. EMBO Rep 2003;4:699–703. [PubMed: 12835756]
16. Senay C, Ferrari P, Rocher C, Rieger KJ, Winter J, Platel D, Bourne Y. The Mtr2-Mex67 NTF2-like domain complex. Structural insights into a dual role of Mtr2 for yeast nuclear export. J Biol Chem 2003;278:48395–403. [PubMed: 14504280]
17. Li K, Zhao K, Ossareh-Nazari B, Da G, Dargemont C, Marmorstein R. Structural basis for interaction between the Ubp3 deubiquitinating enzyme and its Bre5 cofactor. J Biol Chem 2005;280:29176–85. [PubMed: 15955808]
18. Stewart M, Kent HM, McCoy AJ. Structural basis for molecular recognition between nuclear transport factor 2 (NTF2) and the GDP-bound form of the Ras-family GTPase Ran. J Mol Biol 1998;277:635–46. [PubMed: 9533885]
19. Fribourg S, Braun IC, Izaurralde E, Conti E. Structural basis for the recognition of a nucleoporin FG repeat by the NTF2-like domain of the TAP/p15 mRNA nuclear export factor. Mol Cell 2001;8:645–56. [PubMed: 11583626]
20. Vagin A, Teplyakov A. An approach to multi-copy search in molecular replacement. Acta Crystallogr D Biol Crystallogr 2000;56:1622–4. [PubMed: 11092928]
21. Lamzin VS, Wilson KS. Automated refinement of protein models. Acta Crystallogr D Biol Crystallogr 1993;49:129–47. [PubMed: 15299554]

22. Perrakis A, Sixma TK, Wilson KS, Lamzin VS. wARP: improvement and extension of crystallographic phases by weighted averaging of multiple-refined dummy atomic models. Acta Crystallogr D Biol Crystallogr 1997;53:448–55. [PubMed: 15299911]

23. Winn MD, Isupov MN, Murshudov GN. Use of TLS parameters to model anisotropic displacements in macromolecular refinement. Acta Crystallogr D Biol Crystallogr 2001;57:122–33. [PubMed: 11134934]

24. Orci L, Ravazzola M, Meda P, Holcomb C, Moore HP, Hicke L, Schekman R. Mammalian Sec23p homologue is restricted to the endoplasmic reticulum transitional cytoplasm. Proc Natl Acad Sci U S A 1991;88:8611–5. [PubMed: 1924322]

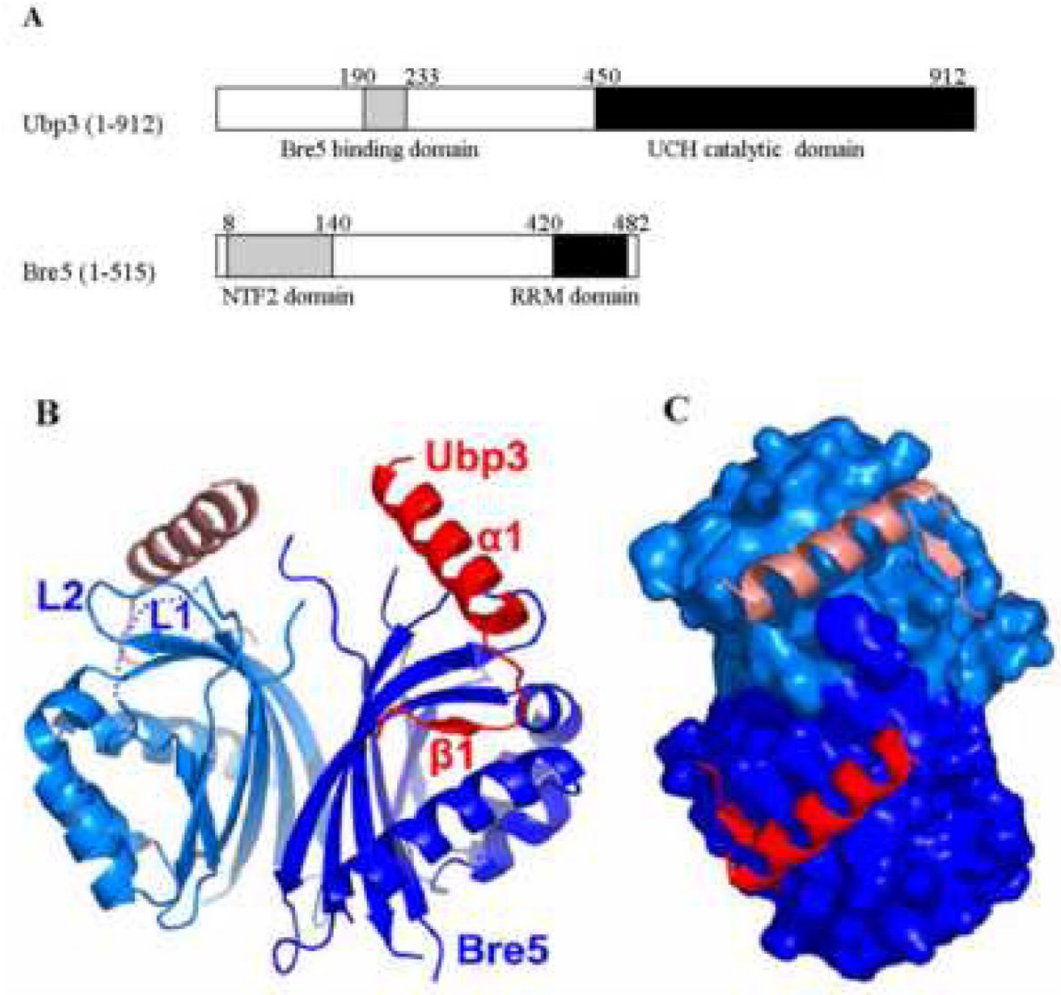

Figure 1. Overall structure of the Ubp3/Bre5 complex

(A) Schematic diagram highlighting the domain structure of the Ubp3 and Bre5 proteins. The grey shaded boxes depict the N-terminal region of Ubp3 and the NTF2-like domain of Bre5 that mediate protein-protein intraction. The black bar depicts the catalytic domain of Ubp3 and the Bre5 C-terminal RRM (RNA recognition motif).

(B) Ribbon diagram of the Ubp3-Nterm/Bre5-NTF2 heterotetramer complex with the two subunits of Bre5 color-coded in light and dark blue, and the two Ubp3 subunits color-coded in red and pink.

(C) Surface representation of the Bre-NTF2 dimer with the Ubp3-Nterm subunits shown in ribbon representation. The view is looking from the top of (A).

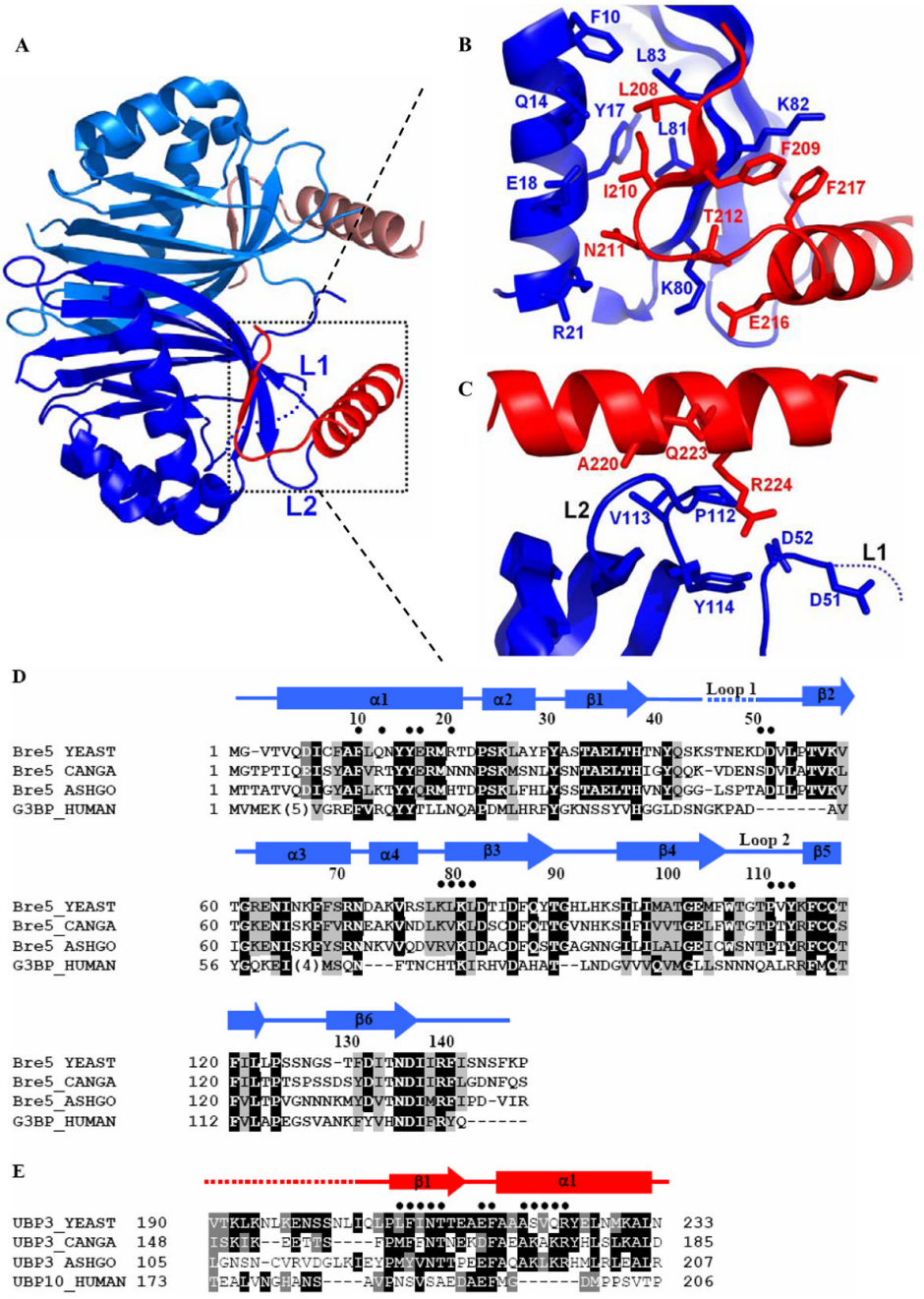

Figure 2. The Ubp3/Bre5 interface

(A) The complex is shown in ribbon representation with the Bre5 regions that mediate Ubp3 interactions highlighted in a dotted box.

(B) Blow-up of Ubp3 β1-turn interactions with Bre5. Side chains that mediate Ubp3-Bre5 van der Waals interactions are included.

(C) Blow-up of Ubp3 α1-helix interactions with Bre5. Side chains that mediate Ubp3-Bre5 van der Waals interactions are included.

(D) Sequence alignment of yeast and human Bre5 homologues within the NTF2-like domain. Strictly conserved residues are shaded in black and conservative substitutions are shaded in grey. Secondary structural elements of S. cerivisea Bre5 are indicated above the sequence

alignment and a solid circle above the sequence alignment donates residues that participate in Ubp3 interactions. The dotted line indicates regions of disorder in the crystal structure. **(E)** Sequence alignment of yeast and human Ubp3 homologues in the N-terminal Bre5 interaction region. Shading and secondary structure are indicated as described above and solid circles above the sequence alignment donates Ubp3 residues that participate in Bre5 interactions.

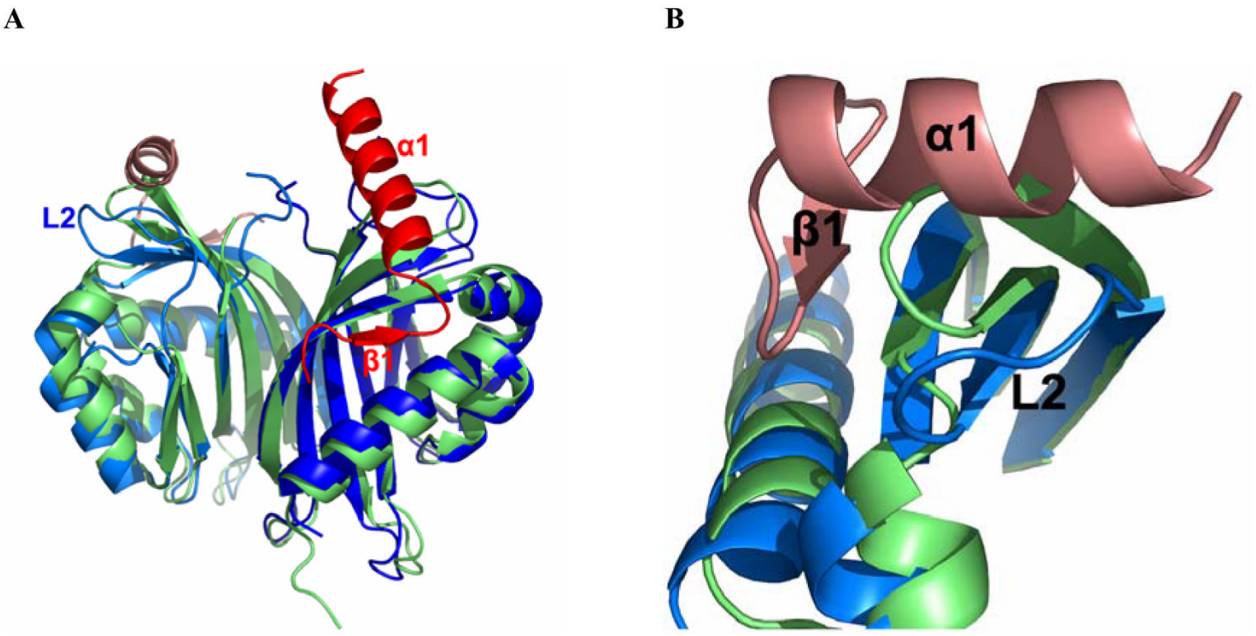

Figure 3. Comparison between Ubp3-bound and free Bre5-NTF2 domain

(A) Ribbons comparison of the free Bre5-NTF2 domain (green) with the Bre5-NTF2 domain in complex with Ubp3 (blue).

(B) A blow-up view looking from the top of (A).

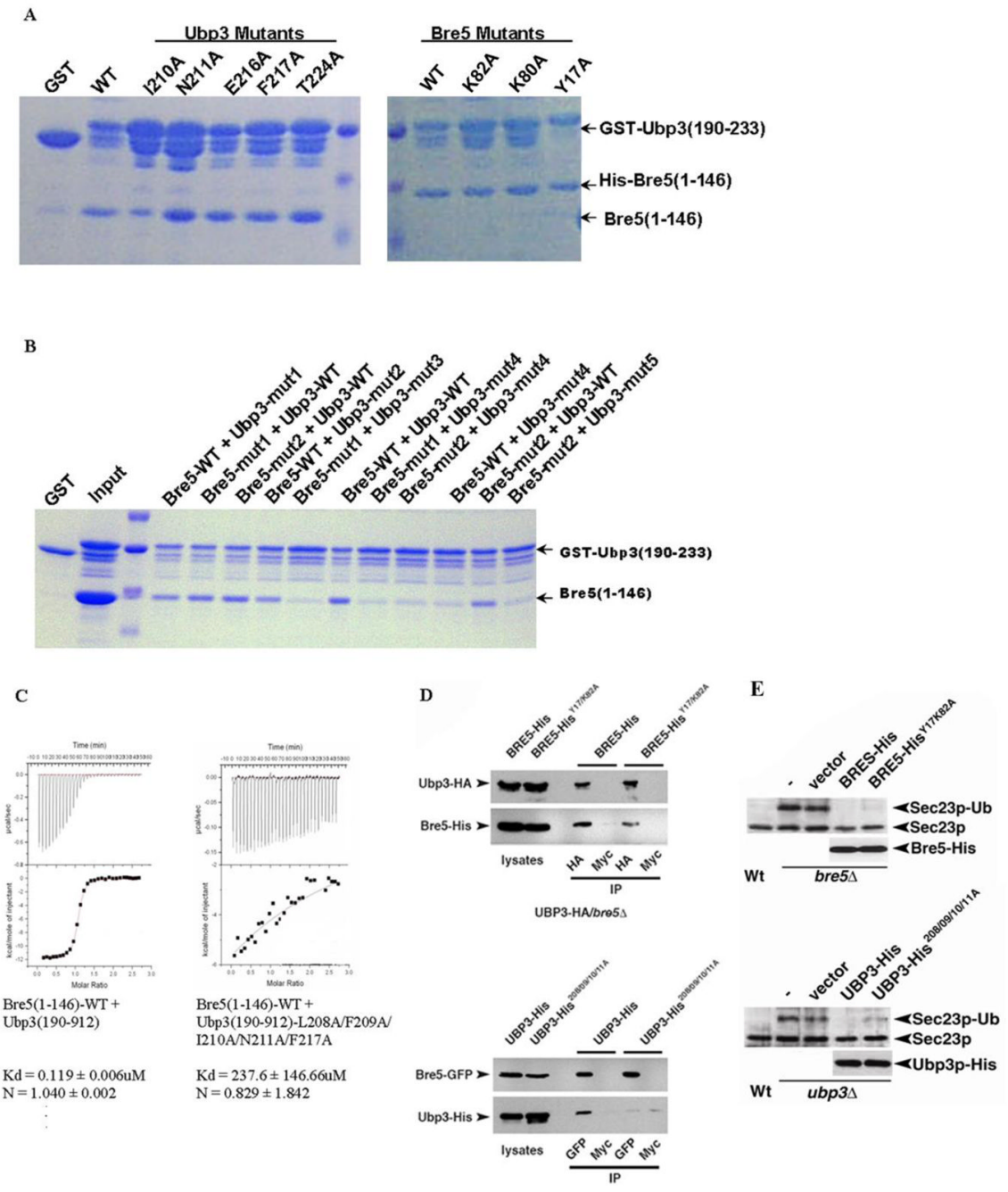

Figure 4. Bre5-Ubp3 binding studies using wild-type and mutant proteins

(A) SDS-PAGE gel of GST pull-down results with wild-type and single-alanine mutants of Bre5 and Ubp3.

(B) SDS-PAGE gel of GST pull-down results with wild-type and multiple-alanine mutants of Bre5 and Ubp3. The mutations indicated above the gel are as follows: Bre5 mut1-Y17A/K82A, mut2-Y17A/K80A/K82A; Ubp3 mut1-L208A/F209A, mut2-I210A/F217A, mut3-N211A/F217A, mut4-L208A/F209A/I210A/N211A, mut5-L208A/F209A/I210A/N211A/F217A.

(C) Binding isotherms for Isothermal Titration Calorimetry (ITC) runs in which wild type Bre5 (1–146) is titrated with wild-type Ubp3(189–912). Data from one of the duplicate runs is shown. The area under each injection spike (above) is integrated and fitted using non-linear

least squares regression analysis (below). The calculated dissociation constant (K_d) and stochiometry (N) is indicated below the respective curve.

(D) UBP3-HA/bre5Δ (upper panel) or BRE5-GFP/ubp3Δ (lower panel) cells were transformed with vector expressing His-tagged version of wild-type BRE5 (BRE5-His), UBP3 (UBP3-HA), BRE5 or UBP3 in which the indicated residues have been mutated to Ala (BRE5-His$^{Y17/K82A}$ or UBP3-His$^{208/209/210/211A}$). Lysates were immunoprecipitated using the indicated antibodies and analyzed by SDS-PAGE and Western-blotting. Immunoprecipitation with anti-myc antibodies was used as a negative control.

(E) SDS-PAGE analysis and Western blotting of extracts from Bre5Δ cells or Ubp3Δ cells transformed with vector expressing His-tagged versions of wild-type Bre5 (Bre5-His), Ubp3 (Ubp3-His), Bre5 in which the residues have been mutated to Ala (Bre5-His $^{Y17A/K82A}$) or Ubp3 in which the residues have been mutated to Ala (Ubp3-His $^{208/209/210/211A}$). The Western blotting employed antibodies against ubiquitylated Sec23 (upper panel) or His (lower panel).

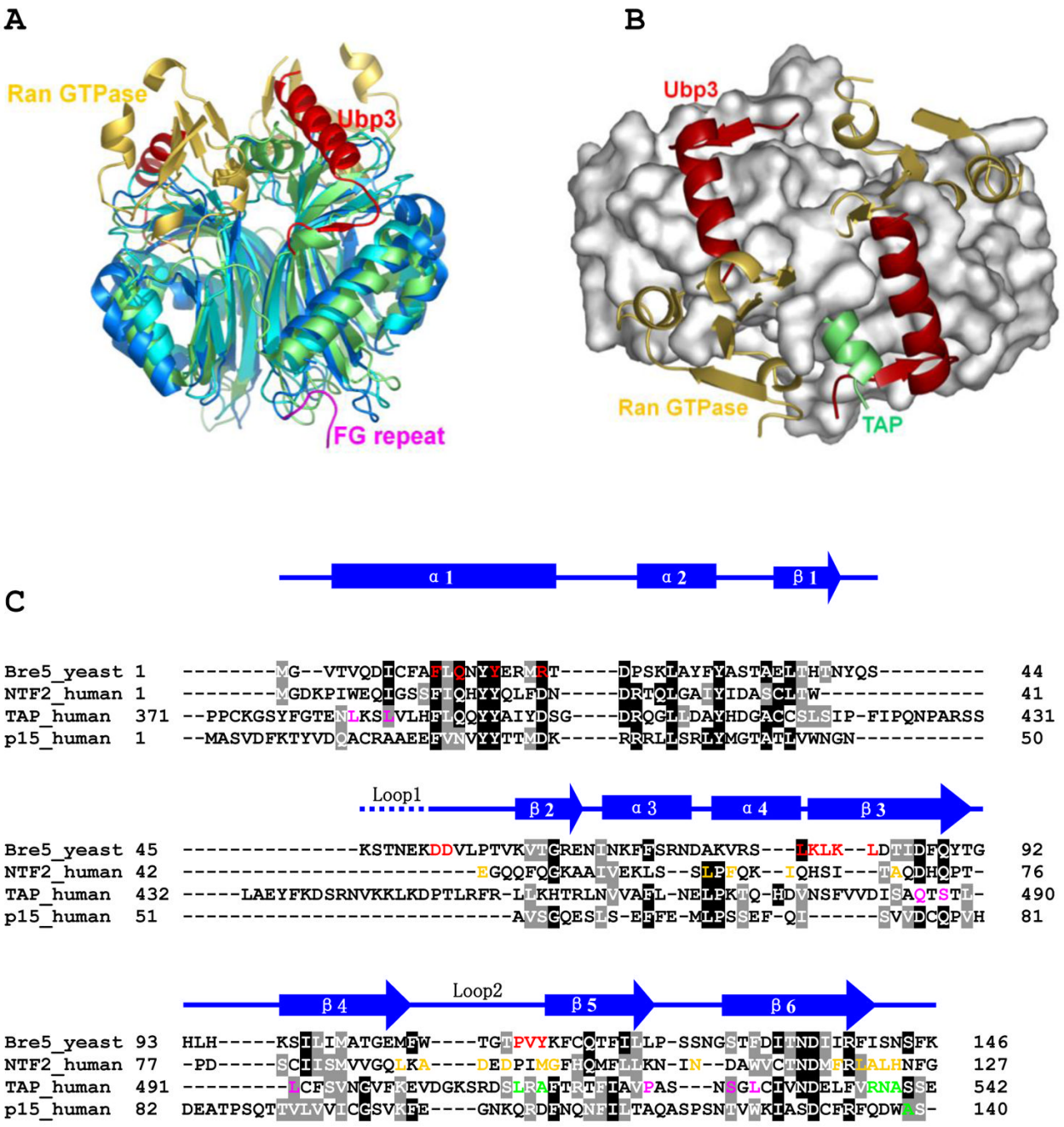

Figure 5. Comparison of the Bre5/Ubp3 complex with other protein complexes with NTF2-like domains

(A) The Bre5/Ubp3 complex (blue and red, respectively) is superimposed in ribbon representation with other protein complexes with NTF2-like domains including the human NTF2/Ran GTPase complex (cyan and orange), the human TAP/P15/FG repeat complex (green and purple).

(B) A view from the top of (A). Only the NTF2-like domain of the Bre5 dimer is shown (in surface representation) for clarity.

(C) Sequence alignment of the Bre5 NTF2–like domain with NTF2 and other NTF2-like domains in (A). Strictly conserved residues are shaded in black and conservative substitutions

are shaded in grey. Secondary structural elements of *S. cerivisea* Bre5 are indicated above the sequence alignment and the dotted line indicates regions of disorder in the crystal structure of Bre5-NTF2 in the Ubp3 complex. Residues that have been shown to participate in protein interaction are color-coded according to the NTF2-like interacting proteins in (A).

Table 1

Data collection and structure refinement statistics.

Data statistics	**Native**
Space group	$P2_12_12_1$
a (Å), *b* (Å), *c* (Å)	59.50, 90.59, 101.05
Wavelength (Å)	0.9176
Resolution Range (Å)	50–1.7
Highest Resolution Shell	1.75–1.69
Unique reflections	59376
Completeness (%)[a]	97.4 (91.5)
Multiplicity	3.9
I/I_o	39.1 (3.2)
R_{merge}(%)[b]	3.1 (37.1)
Refinement statistics	
Resolution (Å)	50–1.7
R_{free} (%)[b]	22.5
Rworking (%)	19.6
Number of protein atoms/B-factors (Å^2)	2103/33.2
Number of water atoms/B-factors (Å^2)	146/42.9
R.m.s. deviations	
Bond length (Å)	0.012
Bond angle (°)	1.5
Ramachandran plot	
Residues in most favored regions	259
Residues in additional allowed regions	21
Residues in generously allowed region	0
Residues in disallowed regions	0

[a] values in parentheses are from the highest resolution shell

[b] $R_{merge} = \Sigma|I - \langle I \rangle|/\Sigma\langle I \rangle$

[c] $R_{working} = \Sigma||F_o| - |F_c||/\Sigma|F_o|$

[d] $R_{free} = \Sigma_T||F_o| - |F_c||/\Sigma^b{}_T|F_o|$ [where T is a test data set of 10% for of the total reflections randomly chose and set aside prior to refinement]

Table 2

Summary of GST pull-down studies with wild-type and mutant Bre5 and Ubp3 proteins.

Bre5 Mutations	Ubp3 (WT)	Ubp3 (I210/A)	Ubp3 Mutations	Bre5 (WT)
WT	+ + +	+ +	WT	+ + +
			I210A	+ +
Y17A	+ + +	+ +	N211A	+ + +
			T212A	+ + +
K80A	+ + +	+	E216A	+ + +
			F217A	+ + +
K82A	+ + +	+/−	R224A	+ + +
			L208A/F209A (mut1)	+/−
E105A	+ + +	+ +	I210A/F217A (mut2)	+/−
			N211A/F217A (mut3)	+
Y17A/K82A (mut1)	+ +	+/−	L208A/F209A/I210A/N2 11A (mut4)	+/−
Y17A/K80A/K 82A (mut2)	+ +	+/−	L208A/F209A/I210A/N2 11A/F217 (mut5)	−

+++ wild-type binding;

++ 60–80% of wild type binding;

+ 40–60% of wild type binding;

+/− 20–40% of wild type binding;

− 0–20% of wild type binding.